

# Miniaturised multi-plane light converters via laser-written geometric phase holograms

Unė G. Būtaitė,<sup>1,\*</sup> Martynas Beresna,<sup>2</sup> and David B. Phillips<sup>1,†</sup>

<sup>1</sup>*Physics and Astronomy, University of Exeter, Exeter, EX4 4QL, UK.*

<sup>2</sup>*Optoelectronics Research Centre, University of Southampton, Southampton, SO17 1BJ, UK.*

Multi-plane light converters (MPLCs) are an emerging 3D beam shaping technology capable of deterministically mapping a basis of input spatial light modes to a new basis of output modes. The ability to perform such spatial reformatting operations has many future applications in both classical and quantum photonics, spanning from optical communications to photonic computing and imaging. MPLCs are intricate optical systems consisting of a cascade of inverse-designed diffractive optical elements, typically separated by free-space. In this work we investigate the fabrication of miniaturised fully-encapsulated transmissive MPLCs within a glass chip using single-step direct laser writing. Our approach relies on the formation of femto-second laser induced birefringent nanogratings with a spatially controllable fast axis orientation. The glass chip is internally patterned with layers of these nanogratings to create multiple geometric phase holograms which imprint controllable phase patterns onto circularly polarised light propagating through them. We experimentally demonstrate two proof-of-concept glass-embedded  $700 \times 700 \times 2000 \mu\text{m}^3$  MPLCs: a 3-mode and a 10-mode Hermite-Gaussian mode sorter. We discuss the fabrication challenges and future improvements of these devices. Our work plots a path towards the rapid prototyping of robust monolithic MPLC technology.

The spatio-temporal amplitude, phase and polarisation texture of light carries numerous independent degrees-of-freedom, representing an exceptionally high information capacity. Tapping into this resource by gaining full control over all of light's dimensions is a long standing challenge in photonics [1–3]. In particular, the ability to individually address specific degrees-of-freedom within optical fields, while leaving the other degrees-of-freedom unperturbed, is crucial to unlocking the full potential of photonic technologies [4]. While techniques to manipulate optical fields based on their spectral or polarisation properties are relatively mature, fine control over the *spatial* dimensions within light fields currently lags behind. A key operation is that of a *spatial mode sorter*: an optical system capable of passively decomposing an incident light field into a basis of transverse spatial light modes, and redirecting the energy carried by each mode to separate locations at the output [5].

Multi-plane light conversion is an emerging technology that can tackle this problem [6–11]. A multi-plane light converter (MPLC) – more recently coined as a linear *diffractive neural network* [12, 13] – consists of a cascade of diffractive optical elements that are separated by free-space, as shown in Fig. 1(a). The spatially-varying phase profiles of these phase masks are crafted through the process of inverse design [14] to solve a particular spatial manipulation task at hand. The optical field flowing through an MPLC is imprinted with the phase pattern of each plane in turn, while diffraction through the space between the planes serves to exchange energy laterally. In this way, input optical fields are gradually transformed into the desired output fields as they flow through the device. Crucially, in contrast to single-plane devices such as individual spatial light modulators (SLMs) or metasurfaces which can typically only efficiently transform a *single* input mode at

a time [15–17], MPLCs can efficiently process multiple different input modes in parallel, thus – in principle – achieving near arbitrary spatial reformatting operations.

The versatility of multi-plane light conversion has been exploited to achieve a variety of spatial mode sorters. Notably, sorting up to 1000 Hermite-Gaussian (HG) or Laguerre-Gaussian (LG) modes has been demonstrated [18]. MPLCs have also been applied to sort Zernike modes and ‘random’ modes formed from orthogonal sets of speckle patterns [19]. Beyond mode sorting, more general spatial transformations, basis rotations and arbitrary linear optical circuits are also made possible with this technology [20, 21]. These developments promise a range of emerging photonic applications. MPLCs and mode sorters can act as spatial mode multiplexers for space division multiplexing in optical communications [22–24]; they underpin quantum-optimal far-field super-resolution imaging [25] and exoplanet detection [26]; they can be deployed to reverse the spatial scrambling effects of multimode optical fibres [27–29] and opaque scattering media [30, 31]; they can realise passive all-optical matrix multiplication for low-energy linear optical computing [32, 33], and have applications to optical neural networks [34] and as unitary operators for future quantum computing paradigms [10, 35–37].

Given the complexity of MPLCs, a major challenge is their accurate physical construction. Various methods are under development. So far, reconfigurable MPLCs have been realised using multiple reflections on SLMs [8, 9, 21, 28, 38]. Fixed compact reflective MPLCs have been fabricated via lithographically etched diffraction gratings [4, 11] or metasurfaces [39, 40]. Transmissive MPLCs and multispectral and polarimetric sorters have been fabricated using two photon polymerisation (2PP) 3D printing [41–43]. Laser writing directly within glass has also been used to engineer binary aperiodic volume optics that offer similar functionality to MPLCs [44–46].

\* [u.butaite@exeter.ac.uk](mailto:u.butaite@exeter.ac.uk)

† [d.phillips@exeter.ac.uk](mailto:d.phillips@exeter.ac.uk)

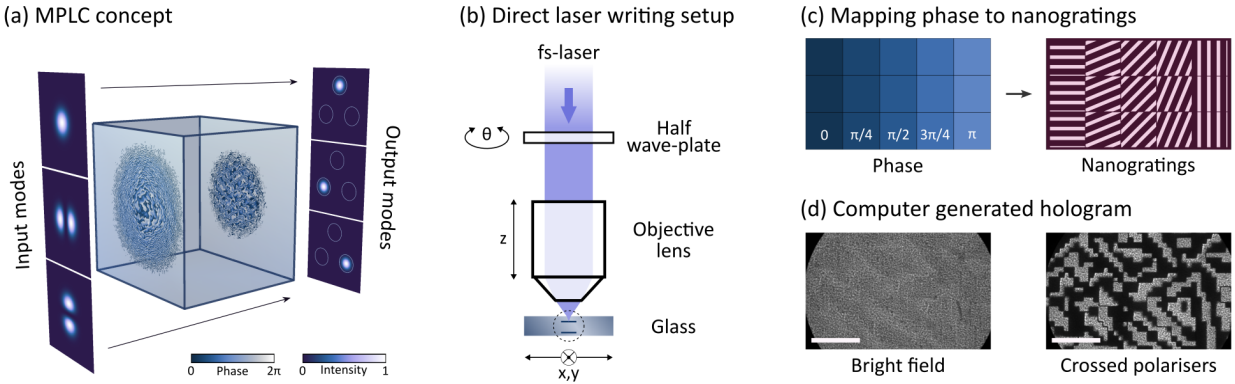


**FIG. 1. Concept.** (a) A schematic of a monolithic 2-plane MPLC laser-written inside a silica glass chip. Here the MPLC is shown sorting the energy carried by 3 HG transverse spatial modes incident from the left into focussed spots in different locations on the right. In our experiments the incident and output spatial modes are centred on a common axis – they are shown displaced vertically here for clarity. The two inverse-designed phase planes are visible inside the glass chip. (b) A schematic of our custom-built direct laser writing system to fabricate miniaturised MPLCs. The incoming fs-beam is linearly polarised. A half wave-plate held in a motorized rotation mount controls the orientation ( $\theta$ ) of the linear polarisation of the beam, after which the beam is focussed into the glass substrate by an objective lens. The glass is translated relative to the writing beam using 3D translation stages whose motion (along Cartesian directions  $x$ ,  $y$ , and  $z$ ) is synchronised with the laser emission and the HWP orientation. (c) Our MPLC inverse-design algorithm yields the optimised phase profiles for each plane, and this is then mapped to the writing orientation of the nanogratings, which corresponds to the local fast-axis of the geometric phase holograms. (d) 60X optical images of a laser-written geometric phase hologram: in bright field and imaged through two crossed linear polarisers. The hologram has 4 phase levels, although it appears binary when imaged between crossed polarisers. Here the pixel size is 10  $\mu\text{m}$ , and the scale bar is 100  $\mu\text{m}$ .

### MPLCs via cascaded geometric phase holograms

In this work we explore the feasibility of fabricating transmissive MPLCs within a glass chip by laser-writing cascaded geometric phase holograms. This approach offers the possibility of creating compact monolithic millimetre-scale MPLCs via a single-step process requiring no post-fabrication plane-to-plane alignment steps. We experimentally demonstrate proof-of-concept glass-embedded MPLCs, of  $<0.8 \text{ mm}^3$  in volume, inverse-designed to sort up to 10 HG modes, and discuss the fabrication challenges and future improvements of these devices. These results were first presented at *Photon 2024*, the Institute of Physics (UK) conference on optics and photonics [47].

Figure 1 illustrates our concept. Each phase mask is fabricated by generating fs-laser induced birefringent nanogratings within high-purity silica glass [48–51]. The fast-axis orientation of these birefringent structures is controlled by the orientation of the linear polarisation state of the writing beam [52]. By rotating the orientation of these nanogratings as a function of position, it is possible to laser-fabricate geometric phase holograms which act as half wave-plates with a spatially-varying fast-axis orientation [53, 54]. When illuminated with a circularly polarised readout beam, the transmitted light picks up a spatially-varying geometric phase (also known as a Pancharatnam-Berry phase [55–57]), dictated by the pattern in the fast-axis orientation imprinted across the hologram. Simultaneously, the handedness of the transmitted circularly polarised beam is flipped. In this way, pixelated phase patterns are imprinted onto incident beams as they propagate through the geometric phase holograms. Creating layers of these structures within a single

glass chip using fs-laser writing (as illustrated in Fig. 1(b)), inverse-designed to perform a given light processing task, results in a fully encapsulated miniaturised MPLC acting on transverse spatial modes with a specified handedness of circular polarisation [47].

The relationship between the desired phase and nanograting orientation can be understood via Jones calculus, where a transverse electric field vector is represented by a Jones vector describing the amplitude and phase of the two electric field components in Cartesian coordinates. If left-circularly polarised light  $|L\rangle$  passes through a nanograting half wave-plate, described by a Jones matrix  $H$ , with its fast axis oriented at an angle  $\phi$ , we have:

$$H|L\rangle = \begin{bmatrix} \cos(2\phi) & \sin(2\phi) \\ \sin(2\phi) & -\cos(2\phi) \end{bmatrix} \begin{bmatrix} 1 \\ i \end{bmatrix} = \begin{bmatrix} e^{i2\phi} \\ -ie^{i2\phi} \end{bmatrix} = |R\rangle e^{i2\phi}. \quad (1)$$

We see that left-circularly polarised light gets converted into right-circularly polarised light  $|R\rangle$  whilst simultaneously picking up a phase of  $2\phi$ . This illustrates how the geometric phase emerges from the orientation of the nanograting pixels that make up a phase plane, as depicted in Fig. 1(c).

### Results

We begin by optimising the laser-writing parameters to create a single geometric phase hologram designed to transform an incident circularly polarised Gaussian beam of wavelength 633 nm into an image projected into the far-field [53, 54]. Methods gives details of our custom-built fs-laser-writing platform and the fabrication process. The geometric phase hologram is 1  $\text{mm}^2$  in area, with a resolution of

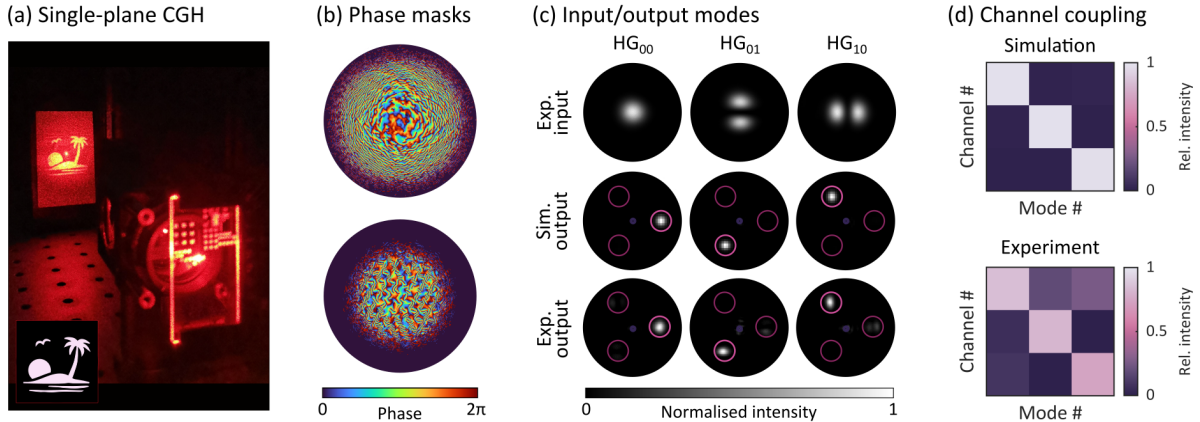


**FIG. 2. Laser-written computer generated hologram and 3-mode HG mode sorter.** (a) Demonstration of a single laser-written  $1 \times 1 \text{ mm}^2$  geometric phase hologram designed to project an image (tropical island scene – target image shown in inset) into the far-field. We see the glass slide patterned with various laser-written test structures in the foreground. The hologram under test is illuminated with a Gaussian beam, and the image is projected onto a piece of white card in the background, after passing through a polarisation filter. (b) Jointly inverse-designed phase profiles of the two planes of the 3-mode HG mode sorter. Upper panel: first hologram; Lower panel: second hologram. (c) Top row: experimentally measured intensity images of input HG modes; Middle row: simulated far-field outputs of ideal 3-mode HG mode sorter; Bottom row: experimentally measured outputs of the laser-written sorter. The location of the output channels is marked by pink circles, with the target output channel highlighted; the central violet circle marks the point around which the channels are arranged. (d) Simulated and experimentally measured coupling matrices describing the relative intensity transmitted into each output channel as the MPLC is illuminated with each input mode in turn. The sum of each column is normalised to 1. The mean off-diagonal intensity value of the simulated [experimental] coupling matrix is 0.02 [0.2].

500  $\times$  500 pixels (i.e. a pixel pitch of 2  $\mu\text{m}$ ). The phase pattern, also referred to as a computer generated hologram (CHG) was designed using the well-established Gerchberg-Saxton algorithm [58], and rounded to 4 phase levels – chosen as a balance between beam shaping fidelity and laser-writing time (see Methods). To achieve a response close to that of a half wave-plate, within each phase hologram, we write 2 layers of nanogratings vertically spaced by 44  $\mu\text{m}$ .

Figure 2(a) shows the result of illuminating our laser-written single-plane geometric phase hologram with a Gaussian beam of beam diameter of  $\leq 1 \text{ mm}$ . We observe the target image (a tropical island sunset scene in this case) appearing in the far-field of the hologram, atop a low intensity speckled background. We also observe a bright spot in the zero diffraction order, which we measure to contain  $\sim 13\%$  of the energy transmitted to the camera when the opposite handedness of circular polarisation is filtered out. We anticipate that the laser-writing process can be further optimised in terms of efficiency and suppression of zero-order diffraction – see Discussion Section.

We next fabricate a proof-of-concept 2-plane MPLC designed to sort 3 HG modes into focussed spots at different lateral positions, arranged around a ring, in the far-field of the MPLC output. HG mode sorters are finding a growing number of applications, for example as 1D to 2D field transformers for spatio-temporal beam shaping [4, 59] and as spatial multiplexers for space-division multiplexing through graded-index multimode fibres [24].

Inverse design of the phase profiles of each plane is conducted using a custom-written computationally efficient ad-

joint gradient descent algorithm with an objective function designed to optimise the overlap between the target and actual output fields, described in our previous work [19]. Our model is based on scalar diffraction theory under the assumption that the polarisation is uniform across any given plane. We use the angular spectrum method to propagate the fields between the phase masks (which are assumed to be infinitely thin) accounting for the refractive index of silica glass. As before, the pixel pitch is 2  $\mu\text{m}$ . The diameter of each circular hologram is 550  $\mu\text{m}$  and the distance between the holograms is 2 mm, resulting in a total MPLC volume of  $\sim 0.5 \text{ mm}^3$ . Figure 2(b) shows the phase profile of the two holograms. For our proof-of-principle experiments, we also add a linear phase ramp to each hologram to separate the shaped light from the undiffracted 0-order light – an approach also sometimes employed with SLM-based MPLCs [13]. Consequently, the position of the second phase mask is translated sideways by 60  $\mu\text{m}$  in order to align it with the 1<sup>st</sup> diffraction order emanating from the first phase mask. We expect this approach will be unnecessary in more efficient future designs. Finally, in these designs we round the continuous phase distribution to 6 phase levels.

To test our laser-written MPLC, it is crucial to create the input HG transverse spatial modes with high quality, as the MPLC outputs are – by design – highly sensitive to input beam fidelity. To achieve this we use a liquid crystal SLM, aberration-corrected [60], and placed in the Fourier plane of the first MPLC phase mask. The SLM dynamically displays a sequence of phase holograms which are designed to precisely shape both the amplitude and phase of the HG modes

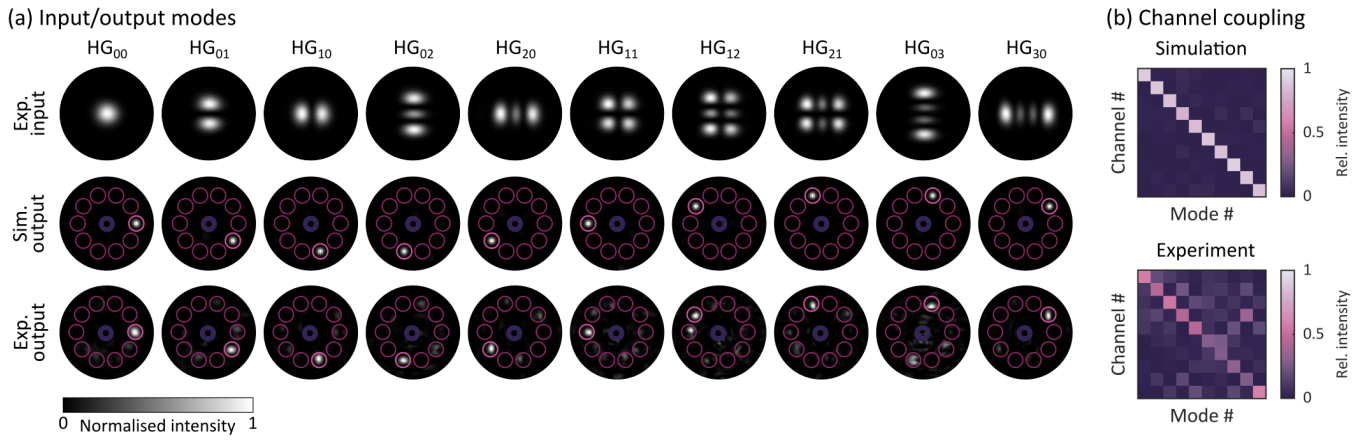


FIG. 3. **10-mode HG mode sorter.** (a) Top row: experimentally measured intensity images of input HG modes; Middle row: simulated far-field outputs of ideal 10-mode HG mode sorter; Bottom row: experimentally measured outputs of the laser-written sorter. The location of the output channels is marked by pink circles, with the target output channel highlighted; the central violet circle marks the point around which the channels are arranged. (b) Simulated and experimentally measured coupling matrices describing the relative intensity transmitted into each output channel as the MPLC is illuminated with each input mode in turn. The sum of each column is normalised to 1. The mean off-diagonal intensity value of the simulated [experimental] coupling matrix is 0.13 [0.58].

incident onto the MPLC [61]. The experimentally measured intensity images of these incident HG modes are shown in the top row of Fig. 2(c). The lower two rows of Fig. 2(c) show a comparison between simulated and experimentally measured far-field outputs when the 3-mode MPLC is illuminated with each of the 3 input HG modes in turn. For each input mode, we observe light predominantly focussed into the correct output channel.

To quantitatively analyse the MPLC performance, Fig. 2(d) shows a comparison between simulated and experimentally measured coupling matrices, describing the relative intensity of light found in each circular output channel when the MPLC is illuminated with each input HG mode. Our proof-of-principle prototype exhibits a higher proportion of undesired mode coupling (i.e., power in off-diagonal elements) in comparison with simulations of an ideal system. Routes for improvement are described in the Discussion Section below.

Finally, we push the mode-capacity limits and complexity of our 2-plane MPLC and inverse-design a 10-mode HG mode sorter. The pixel pitch and axial plane separation are as before, and the hologram diameter is now 700  $\mu\text{m}$ , resulting in a device volume of  $\sim 0.8 \text{ mm}^3$ . Due to the increase in the number of transverse spatial modes, the simulated performance of this 10-mode device is lower than that of the 3-mode HG sorter – this is expected, as MPLCs that control more spatial/spectral modes typically require more phase planes to maintain the same performance [19, 62]. Furthermore, from an experimental perspective, a higher mode capacity results in phase hologram designs of increased complexity (with phase values that vary rapidly across each plane) which present additional challenges to fabricate accurately.

Figure 3(a) shows simulated versus experimentally measured outputs of the 10-mode HG mode sorter when illuminated with all 10 input HG modes in turn. We see

that in most cases power is focussed into the correct output channel, while there is also an increased level of mode coupling in comparison with the 3-mode sorter. Analysing the coupling matrices (Fig. 3(b)), we observe a lower sorting performance for some of the higher order HG modes. In particular, there are greater levels of coupling between the output channels of the HG<sub>02</sub> and HG<sub>03</sub> modes, and the HG<sub>11</sub> and HG<sub>12</sub> modes. This mode-dependent increase in cross-talk is likely due to (i) the fidelity of input mode generation and (ii) the accuracy of the MPLC fabrication itself. For example, higher order transverse spatial modes are more challenging to generate with high fidelity, and more susceptible to small input misalignments. In addition, such higher order modes may be more perturbed by MPLC fabrication imperfections.

## Discussion and conclusions

We have demonstrated the fabrication and testing of proof-of-concept laser-written glass-embedded MPLCs, occupying a volume of  $< 0.8 \text{ mm}^3$  and able to process up to 10 spatial modes simultaneously. The fabrication process automatically co-registers the planes with high-accuracy sample translation stages, reducing post-fabrication alignment challenges. We now assess future avenues of development, and consider our work in the wider context of alternative MPLC fabrication approaches.

*Mode conversion fidelity:* While our proof-of-concept results show promise, it will be necessary to improve the beam shaping fidelity, and suppress levels of modal cross-talk for future applications. Loss of output fidelity can arise from distortion or misalignments in the input beams, and from the MPLC itself. Focussing on the MPLC, fabrication errors cause the physical device to depart from the ideal model. Potential problems include nanograting pixel cross-talk (a phenomenon in which nanogratings that rapidly vary in orientation from pixel-

to-pixel may result in disruption or overwriting of adjacent pixels), the finite thickness of each phase hologram, and errors in hologram separation due to aberrations when laser-writing at depth. Designing more smoothly-varying holograms can go some way to alleviate all of these issues, as this suppresses pixel cross-talk and decreases the range of  $k$ -vectors in light flowing through the device, thus reducing the sensitivity to errors. Careful calibration of the laser-writing process as a function of writing direction [63] and depth [64] will also improve fabrication accuracy. Building a more accurate digital model of the MPLC used in the inverse-design process may further reduce any mismatch between the MPLC design and the physically constructed device. For example, Barré et al. incorporated knowledge of the profile of pre-measured laser-written features into their inverse-design model to maintain a close match to reality [46].

*Light processing efficiency:* A crucial next step is to improve the efficiency of mode conversion. In our present designs, we estimate the efficiency of each plane to be  $\sim 20\%$ , which limits the number of planes that can be fabricated and does not yet reach the efficiency demanded by many applications. Fortunately, previous work has demonstrated that the fabrication of high efficiency geometric phase gratings in glass is possible [54, 65, 66].

There are two main areas to address to enhance the efficiency of the geometric phase holograms: polarisation conversion and scattering losses. Polarisation conversion refers to the fidelity with which each hologram approximates an ideal half wave-plate, which should impart a relative phase difference of  $\pi$  between the two electric field components. If this condition is not met, it leads to incident circularly polarised light being transformed into an elliptically polarised output state. The residual light in the ‘wrong’ handedness polarisation state cannot be filtered out in our monolithic geometry, and so pollutes the system further downstream. Thus, optimising the laser-writing parameters to fabricate high-fidelity half wave-plates, even as their fast-axis is varied spatially, is essential for a laser-written MPLC.

Scattering losses result from uncontrolled scattering of light from nanogratings. Light lost in this way is typically scattered across a wide range of angles, leading to a low intensity background at the output plane. There are two ways forward to suppress this uncontrolled scattering: (i) by optimising the writing parameters to generate nanogratings of higher uniformity, which has been shown to enable transmission of up to 90% in the visible range [54, 65]; (ii) by switching to a recently discovered different class of birefringent glass modification known as Type X, originating from the formation of randomly distributed nanopores in silica glass [66]. Type X modification is reported to provide ultralow scattering loss and up to 99% transmission in the visible. That said, we note that a potential drawback of Type X modifications is the weak birefringence of each laser-written layer, meaning potentially tens of layers are required to create a half wave-plate. This thickness may in turn limit the spatial resolution achievable, leading to less compact devices.

*Vectorial light control:* In this work we have focussed on laser writing half wave-plates that impart geometric phase patterns to uniformly circularly polarised light. More generally, we note that by tuning the laser-writing parameters, other birefringent media can be formed, such as polarisation converters and q-plates [53, 67]. Taking advantage of these features, vectorial laser-written MPLCs may be fabricated, in analogy to those recently demonstrated using encapsulated reflective metasurfaces [40].

*Alternative MPLC construction methods:* Finally, assuming the fidelity and efficiency can be improved as expected, it is pertinent to ask ‘When should one consider using this laser-writing MPLC fabrication method over other approaches?’

Passive MPLCs, such as our laser-written device, draw no power (unlike SLM-based MPLCs) but have their function set at the point of manufacture (with the exception of MPLCs designed to multiplex several different functions when the planes undergo relative motion [68]). Fixed MPLCs suit cases where reconfigurability is not necessary, such as for spatial mode demultiplexing for space division multiplexing augmented by digital signal processing [24]. Passive MPLCs created using optical lithography can benefit from substantially lower levels of loss, achieve a broader spectral bandwidth and a much more compact form factor in comparison with MPLCs based on SLMs. For example, a wafer-scale 14-plane reflective MPLC capable of highly efficient, high-fidelity sorting of 45 HG modes across a 200 nm bandwidth centred on 1550 nm, was recently demonstrated [11]. This device occupies a volume of  $\sim 10 \text{ mm}^3$  (i.e.,  $\sim 0.7 \text{ mm}^3$  per plane, or  $\sim 0.22 \text{ mm}^3$  per mode) and presently stands out as the state-of-the-art in terms of passive MPLC performance and mode capacity in a compact package.

Reflective metasurface-based MPLCs can be equally small-scale [39], but tend to have higher scattering losses and narrower spectral responses than their diffraction grating counterparts. This technology is still developing: low mode capacity mode sorters have been demonstrated so far (sorting 3-6 modes). These solutions have the advantage of simultaneously manipulating both space and polarization degrees-of-freedom independently, and may also offer more spectral control [40].

Transmissive MPLCs, in which light is transmitted through – rather than reflected from – each plane, have the potential to be even more compact [41]. Such devices have recently been fabricated using two photon polymerisation (2PP) 3D printing – a highly versatile technique capable of creating free-standing 3D microstructures. State-of-the-art 2PP MPLCs for the visible have pixel pitches below 1  $\mu\text{m}$  and plane separations reduced to tens of microns, occupying volumes down to  $\sim 0.001 \text{ mm}^3$  [42]. However, at these small scales, accurate fabrication via 2PP becomes very challenging (e.g. due to the precision of the polymerisation process and shrinkage distortion during development), and devices demonstrated so far exhibit relatively low fidelity and high levels of uncontrolled scattering losses. Furthermore, free-standing micro-scale components are also extremely fragile, so will require

encapsulation before deployment in real-world applications.

Femtosecond laser modification of glass sits somewhere between 2PP and lithographic approaches. The single-step fabrication process facilitates rapid prototyping of fully-encapsulated devices by circumventing the need for complex multi-step optical lithography or electron beam etching. The creation of laser-written aperiodic volume optics within glass was first demonstrated by Gerke and Piestun in 2010 [44]. More recently Barré et al. inverse-designed aperiodic volume optics based on disconnected waveguide segments distributed throughout a  $\sim 0.04 \text{ mm}^3$  volume, enabling high-efficiency multiplexing of up to 6 modes by incident angle or wavelength [45, 46]. Our cascaded geometric phase hologram approach, should it be fully optimised, is comparable to this approach.

More broadly, femto-second laser-writing into glass is also compatible with other laser writing modalities such as 3D waveguides and optical interconnects, suggesting the future possibility of flexible integration of laser-written MPLCs and aperiodic volume optics with other photonic components. In summary, we have demonstrated a new approach to create miniaturised MPLCs, which adds to the growing toolbox of techniques to deliver ever more complex photonic components at ever decreasing scales.

We note that during the final stages of the preparation of our manuscript we became aware of a related concept presented at SPIE Photonics West 2026 [69].

## METHODS

### Fs-laser writing platform

Our laser writing platform consists of a fs-pulsed laser source (Light Conversion, Pharos) with a pulse duration of 170 fs and central wavelength of 1030 nm. In this work we use the second harmonic with 200 kHz repetition rate and a 515 nm, central wavelength, which is focussed through an objective lens (Olympus Plan Achromat 10X, 0.25NA) into a fused silica glass sample. Before being focussed, the linearly polarised laser beam passes through a zero-order half wave-plate (HWP) held in a computer controlled motorised rotation mount (Thorlabs PRM1/MZ8), allowing the orientation of the linear polarisation of the writing beam to be set. The laser is synchronised with 3-axis nanopositioning translation stages to control the relative motion between the fabrication laser beam and the glass substrate. Hardware control and synchronisation is accomplished via a custom-written application (Labview and G-code). Lateral sample motion is achieved with an Aerotech ANT130XY direct drive 2-axis nanopositioning stage, and axial motion of the objective lens by an Aerotech ANT130LZS direct drive single-axis stage.

During fabrication, we write from the last plane to the first, i.e., from the bottom of the glass chip to the top. To make sure that the response of each phase plane is close to that of a half wave-plate, each plane is written in two identical layers sepa-

rated by 44  $\mu\text{m}$ . We found this to be a good distance to ensure that the newly written layer does not over-write the layer below it. The first phase plane is written at a depth of  $\sim 170 \mu\text{m}$ , while the second plane is written 2 mm deeper. Each pixel in a phase plane is 2  $\mu\text{m}$  in size and consists of a 2 by 2 grid of ‘points’. Each point receives 30 laser pulses, while the stages translate the sample at 2 mm/s.

Ideally, for high efficiency and fidelity, the phase masks would be written with a high bit depth - by setting the half wave-plate orientation before writing each pixel. However, because of the limited speed of our rotation mount, this process would take a very long time. As a compromise, we therefore choose to round the phase to several values - this decreases diffraction efficiency but allows faster fabrication. During the writing, we set the half wave-plate orientation to correspond to one of the phase values and write all of the pixels with this phase. We then repeat the process for each phase value.

## ACKNOWLEDGEMENTS

DBP acknowledges financial support from the European Research Council (ERC) (ERC Starting grant *PhotUntangle*, no. 804626; and ERC Consolidator grant *ModeMixer*, no. 101170907). DBP and UG thank the Engineering and Physical Sciences Research Council (EPSRC) for financial support (*Photon Management in complex dynamic scattering media*, EP/Z535928/1) and (*A-Meta*, EP/W003341/1). DBP also acknowledges financial support from EPSRC Hub grant (*MetaHub*, UKRI1255).

---

- [1] Halina Rubinsztein-Dunlop, Andrew Forbes, Michael V Berry, Mark R Dennis, David L Andrews, Masud Mansuripur, Cornelia Denz, Christina Alpmann, Peter Banzer, Thomas Bauer, *et al.*, “Roadmap on structured light,” *Journal of Optics* **19**, 013001 (2016).
- [2] Ilaria Cristiani, Cosimo Lacava, Georg Rademacher, Benjamin J Puttnam, Ruben S Luís, Cristian Antonelli, Antonio Mecozzi, Mark Shtaif, Daniele Cozzolino, Davide Bacco, *et al.*, “Roadmap on multimode photonics,” *Journal of Optics* **24**, 083001 (2022).
- [3] Yijie Shen, Qiwen Zhan, Logan G Wright, Demetrios N Christodoulides, Frank W Wise, Alan E Willner, Kai-heng Zou, Zhe Zhao, Miguel A Porras, Andy Chong, *et al.*, “Roadmap on spatiotemporal light fields,” *Journal of Optics* **25**, 093001 (2023).
- [4] Mickael Mounaix, Nicolas K Fontaine, David T Neilson, Roland Ryf, Haoshuo Chen, Juan Carlos Alvarado-Zacarias, and Joel Carpenter, “Time reversed optical waves by arbitrary vector spatiotemporal field generation,” *Nature communications* **11**, 5813 (2020).
- [5] David AB Miller, “Sorting out light,” *Science* **347**, 1423–1424 (2015).

[6] Jean-François Morizur, Lachlan Nicholls, Pu Jian, Seiji Armstrong, Nicolas Treps, Boris Hage, Magnus Hsu, Warwick Bowen, Jiri Janousek, and Hans-A Bachor, “Programmable unitary spatial mode manipulation,” *JOSA A* **27**, 2524–2531 (2010).

[7] Guillaume Labroille, Bertrand Denolle, Pu Jian, Philippe Genevaux, Nicolas Treps, and Jean-François Morizur, “Efficient and mode selective spatial mode multiplexer based on multi-plane light conversion,” *Optics express* **22**, 15599–15607 (2014).

[8] Haiyan Wang and Rafael Piestun, “Dynamic 2d implementation of 3d diffractive optics,” *Optica* **5**, 1220–1228 (2018).

[9] Nicolas K Fontaine, Roland Ryf, Haoshuo Chen, David T Neilson, Kwangwoong Kim, and Joel Carpenter, “Laguerre-gaussian mode sorter,” *Nature communications* **10**, 1–7 (2019).

[10] Florian Brandt, Markus Hiekkämäki, Frédéric Bouchard, Marcus Huber, and Robert Fickler, “High-dimensional quantum gates using full-field spatial modes of photons,” *Optica* **7**, 98–107 (2020).

[11] Nicolas K Fontaine, Yetian Huang, Hanzi Huang, Lauren Dallachiesa, Mikael Mazur, Roland Ryf, Haoshuo Chen, David T Neilson, Mark Earnshaw, Mark Cappuzzo, *et al.*, “Wafer scale fabrication of multi-plane light conversion devices,” in *49th European Conference on Optical Communications (ECOC 2023)*, Vol. 2023 (IET, 2023) pp. 1063–1066.

[12] Xing Lin, Yair Rivenson, Nezih T Yardimci, Muhammed Veli, Yi Luo, Mona Jarrahi, and Aydogan Ozcan, “All-optical machine learning using diffractive deep neural networks,” *Science* **361**, 1004–1008 (2018).

[13] Kaden Bearne, Alexander Duplinskiy, Matthew J Filipovich, and AI Lvovsky, “Diffractive neural networks for mode-sorting with flexible detection regions,” *Optics & Laser Technology* **195**, 114544 (2026).

[14] T Hashimoto, T Saida, I Ogawa, M Kohtoku, Tomohiro Shiba, and Hiroshi Takahashi, “Optical circuit design based on a wavefront-matching method,” *Optics letters* **30**, 2620–2622 (2005).

[15] Graham Gibson, Johannes Courtial, Miles J Padgett, Mikhail Vasnetsov, Valeriy Pas’ko, Stephen M Barnett, and Sonja Franke-Arnold, “Free-space information transfer using light beams carrying orbital angular momentum,” *Optics express* **12**, 5448–5456 (2004).

[16] Tomáš Čižmár and Kishan Dholakia, “Exploiting multimode waveguides for pure fibre-based imaging,” *Nature communications* **3**, 1027 (2012).

[17] Michael Mazilu, Tom Vettenburg, Martin Ploschner, Ewan M Wright, and Kishan Dholakia, “Modal beam splitter: determination of the transversal components of an electromagnetic light field,” *Scientific reports* **7**, 9139 (2017).

[18] Nicolas K Fontaine, Haoshuo Chen, Mikael Mazur, Lauren Dallachiesa, KW Kim, Roland Ryf, David Neilson, and Joel Carpenter, “Hermite-gaussian mode multiplexer supporting 1035 modes,” in *Optical Fiber Communication Conference* (Optical Society of America, 2021) pp. M3D–4.

[19] Hlib Kupianskyi, Simon AR Horsley, and David B Phillips, “High-dimensional spatial mode sorting and optical circuit design using multi-plane light conversion,” *APL Photonics* **8** (2023).

[20] Suraj Goel, Saroch Leedumrongwatthanakun, Natalia Herrera Valencia, Will McCutcheon, Armin Tavakoli, Claudio Conti, Pepijn WH Pinkse, and Mehul Malik, “Inverse design of high-dimensional quantum optical circuits in a complex medium,” *Nature Physics* **20**, 232–239 (2024).

[21] José C A. Rocha, Uné G Bütaitė, Joel Carpenter, and David B Phillips, “Self-configuring high-speed multi-plane light conversion,” *Nature Communications* (2025).

[22] David J Richardson, John M Fini, and Lynn E Nelson, “Space-division multiplexing in optical fibres,” *Nature photonics* **7**, 354–362 (2013).

[23] Nicolas K Fontaine, Joel Carpenter, Simon Gross, Sergio Leon-Saval, Yongmin Jung, David J Richardson, and Rodrigo Amezcua-Correa, “Photonic lanterns, 3-d waveguides, multi-plane light conversion, and other components that enable space-division multiplexing,” *Proceedings of the IEEE* **110**, 1821–1834 (2022).

[24] Georg Rademacher, Ruben S Luís, Benjamin J Puttnam, Nicolas K Fontaine, Mikael Mazur, Haoshuo Chen, Roland Ryf, David T Neilson, Daniel Dahl, Joel Carpenter, *et al.*, “3.56 peta-bit/s c+1 band transmission over a 55-mode multi-mode fiber,” in *49th European Conference on Optical Communications (ECOC 2023)*, Vol. 2023 (IET, 2023) pp. 9–12.

[25] Clémentine Rouvière, David Barral, Antonin Grateau, Ilya Karuseichyk, Giacomo Sorelli, Mattia Walschaers, and Nicolas Treps, “Ultra-sensitive separation estimation of optical sources,” *Optica* **11**, 166–170 (2024).

[26] Nico Deshler, Itay Ozer, Amit Ashok, and Saikat Guha, “Experimental demonstration of a quantum-optimal coronagraph using spatial mode sorters,” *Optica* **12**, 518–529 (2025).

[27] Uné G Bütaitė, Hlib Kupianskyi, Tomáš Čižmár, and David B Phillips, “How to build the “optical inverse” of a multimode fibre,” *Intelligent Computing* (2022).

[28] Hlib Kupianskyi, Simon AR Horsley, and David B Phillips, “All-optically untangling light propagation through multimode fibers,” *Optica* **11**, 101–112 (2024).

[29] Haoyi Yu, Zihao Huang, Simone Lamon, Baokai Wang, Haibo Ding, Jian Lin, Qi Wang, Haitao Luan, Min Gu, and Qiming Zhang, “All-optical image transportation through a multimode fibre using a miniaturized diffractive neural network on the distal facet,” *Nature Photonics* , 1–8 (2025).

[30] Sungsam Kang, Yongwoo Kwon, Hojun Lee, Seho Kim, Jin Hee Hong, Seokchan Yoon, and Wonshik Choi, “Tracing multiple scattering trajectories for deep optical imaging in scattering media,” *Nature communications* **14**, 6871 (2023).

[31] Anat Levin and Marina Alterman, “Understanding multi-layered transmission matrices,” in *Proceedings of the Computer Vision and Pattern Recognition Conference* (2025) pp. 23164–23173.

[32] Ravindra A Athale and William C Collins, “Optical matrix-matrix multiplier based on outer product decomposition,” *Applied optics* **21**, 2089–2090 (1982).

[33] Hailong Zhou, Jianji Dong, Junwei Cheng, Wenchan Dong, Chaoran Huang, Yichen Shen, Qiming Zhang, Min Gu, Chao Qian, Hongsheng Chen, *et al.*, “Photonic matrix multiplication lights up photonic accelerator and beyond,” *Light: Science & Applications* **11**, 30 (2022).

[34] Ali Momeni, Babak Rahmani, Benjamin Scellier, Logan G Wright, Peter L McMahon, Clara C Wanjura, Yuhang Li, Anas Skalli, Natalia G Berloff, Tatsuhiko Onodera, *et al.*, “Training of physical neural networks,” *Nature* **645**, 53–61 (2025).

[35] Ohad Lib, Kfir Sulinay, and Yaron Bromberg, “Processing entangled photons in high dimensions with a programmable light converter,” *Physical Review Applied* **18**, 014063 (2022).

[36] Ohad Lib and Yaron Bromberg, “Resource-efficient photonic quantum computation with high-dimensional cluster states,” *Nature Photonics* , 1–7 (2024).

[37] Suraj Goel, Bohnishikha Ghosh, and Mehul Malik, “Quantum information processing with spatially structured light,” *Ad-*

vanced Photonics **8**, 014005–014005 (2026).

[38] Niyazi Ulas Dinc, Mustafa Yildirim, Ilker Oguz, Christophe Moser, and Demetri Psaltis, “Multicasting optical reconfigurable switch,” arXiv preprint arXiv:2401.14173 (2024).

[39] Jaewon Oh, Kangmei Li, Jun Yang, Wei Ting Chen, Ming-Jun Li, Paulo Dainese, and Federico Capasso, “Adjoint-optimized metasurfaces for compact mode-division multiplexing,” ACS photonics **9**, 929–937 (2022).

[40] Go Soma, Kento Komatsu, Yoshiaki Nakano, and Takuo Tanemura, “Complete vectorial optical mode converter using multi-layer metasurface,” Nature Communications **16**, 7744 (2025).

[41] Xavier Porte, Niyazi Ulas Dinc, Johnny Moughames, Giulia Panusa, Caroline Juliano, Muamer Kadic, Christophe Moser, Daniel Brunner, and Demetri Psaltis, “Direct (3+ 1) d laser writing of graded-index optical elements,” Optica **8**, 1281–1287 (2021).

[42] Qian Zhang, Haoyi Yu, Jie Zhang, Yuedi Zhang, Chao Meng, Jiali Sun, Yu Miao, Qiming Zhang, Min Gu, and Juergen W Czarske, “Demultiplexing through a multimode fiber using chip-scale diffractive neural networks,” arXiv preprint arXiv:2512.04767 (2025).

[43] Gregory Roberts, Conner Ballew, Tianzhe Zheng, Juan C Garcia, Sarah Camayd-Muñoz, Philip WC Hon, and Andrei Faraon, “3d-patterned inverse-designed mid-infrared metaoptics,” Nature Communications **14**, 2768 (2023).

[44] Tim D Gerke and Rafael Piestun, “Aperiodic volume optics,” Nature photonics **4**, 188–193 (2010).

[45] Nicolas Barré and Alexander Jesacher, “Inverse design of gradient-index volume multimode converters,” Optics Express **30**, 10573–10587 (2022).

[46] Nicolas Barré, Ravi Shivaraman, Simon Moser, Patrick Salter, Michael Schmidt, Martin J Booth, and Alexander Jesacher, “Direct laser-written aperiodic photonic volume elements for complex light shaping with high efficiency: inverse design and fabrication,” Advanced Photonics Nexus **2**, 036006–036006 (2023).

[47] Unė G Būtaitė, Martynas Beresna, and David B Phillips, “Photon 2024, institute of physics (uk) conference on optics and photonics,” (2024).

[48] Yasuhiko Shimotsuma, Peter G Kazansky, Jiarong Qiu, and Kazuoki Hirao, “Self-organized nanogratings in glass irradiated by ultrashort light pulses,” Physical review letters **91**, 247405 (2003).

[49] VR Bhardwaj, E Simova, PP Rajeev, C Hnatovsky, RS Taylor, DM Rayner, and PB Corkum, “Optically produced arrays of planar nanostructures inside fused silica,” Physical review letters **96**, 057404 (2006).

[50] Yves Bellouard, E Barthel, AA Said, M Dugan, and Ph Bado, “Scanning thermal microscopy and raman analysis of bulk fused silica exposed to low-energy femtosecond laser pulses,” Optics Express **16**, 19520–19534 (2008).

[51] Sören Richter, Matthias Heinrich, Sven Döring, Andreas Tünnermann, Stefan Nolte, and Ulf Peschel, “Nanogratings in fused silica: Formation, control, and applications,” Journal of Laser Applications **24** (2012).

[52] Martynas Beresna, Mindaugas Gecevičius, and Peter G Kazansky, “Ultrafast laser direct writing and nanostructuring in transparent materials,” Advances in Optics and Photonics **6**, 293–339 (2014).

[53] Martynas Beresna, Mindaugas Gecevičius, Peter G Kazansky, and Titas Gertus, “Radially polarized optical vortex converter created by femtosecond laser nanostructuring of glass,” Applied Physics Letters **98** (2011).

[54] Rokas Drevinskas and Peter G Kazansky, “High-performance geometric phase elements in silica glass,” APL Photonics **2** (2017).

[55] Shivaramakrishnan Pancharatnam, “Generalized theory of interference, and its applications: Part i. coherent pencils,” in *Proceedings of the Indian Academy of Sciences-Section A*, Vol. 44 (Springer, 1956) pp. 247–262.

[56] Michael Victor Berry, “Quantal phase factors accompanying adiabatic changes,” Proceedings of the Royal Society of London. A. Mathematical and Physical Sciences **392**, 45–57 (1984).

[57] Jeeva Anandan, “The geometric phase,” Nature **360**, 307–313 (1992).

[58] Guo-zhen Yang, Bi-zhen Dong, Ben-yuan Gu, Jie-yao Zhuang, and Okan K Ersoy, “Gerchberg–saxton and yang–gu algorithms for phase retrieval in a nonunitary transform system: a comparison,” Applied optics **33**, 209–218 (1994).

[59] Andrew V Komonen, Nicolas K Fontaine, Martin Plöschner, Marcos Maestre Morote, David T Neilson, Joel Carpenter, and Mickael Mounaix, “Programmable spatiotemporal oam optical toroidal beams with completely tunable properties,” arXiv preprint arXiv:2506.20365 (2025).

[60] Tomáš Čižmár, Michael Mazilu, and Kishan Dholakia, “In situ wavefront correction and its application to micromanipulation,” Nature Photonics **4**, 388–394 (2010).

[61] Jeffrey A Davis, Don M Cottrell, Juan Campos, María J Yzuel, and Ignacio Moreno, “Encoding amplitude information onto phase-only filters,” Applied optics **38**, 5004–5013 (1999).

[62] Vincent Girouard and Nicolás Quesada, “Near-optimal decomposition of unitary matrices using phase masks and the discrete fourier transform,” Journal of the Optical Society of America B **43**, A66–A73 (2025).

[63] Mindaugas Gecevičius, Martynas Beresna, Jingyu Zhang, Weijia Yang, Hiromichi Takebe, and Peter G Kazansky, “Extraordinary anisotropy of ultrafast laser writing in glass,” Optics express **21**, 3959–3968 (2013).

[64] PS Salter, M Baum, I Alexeev, M Schmidt, and MJ Booth, “Exploring the depth range for three-dimensional laser machining with aberration correction,” Optics express **22**, 17644–17656 (2014).

[65] Takaumi Ohfuchi, Yuya Yamada, Masaaki Sakakura, Naoaki Fukuda, Toshio Takiya, Yasuhiko Shimotsuma, and Kiyotaka Miura, “The characteristic of birefringence and optical loss in femtosecond-laser-induced region in terms of nanogratings distribution,” Journal of Laser Micro Nanoengineering **12**, 217–221 (2017).

[66] Masaaki Sakakura, Yuhao Lei, Lei Wang, Yan-Hao Yu, and Peter G Kazansky, “Ultralow-loss geometric phase and polarization shaping by ultrafast laser writing in silica glass,” Light: Science & Applications **9**, 15 (2020).

[67] Lorenzo Marrucci, Carlo Manzo, and Domenico Paparo, “Optical spin-to-orbital angular momentum conversion in inhomogeneous anisotropic media,” Physical review letters **96**, 163905 (2006).

[68] Haiyan Wang and Rafael Piestun, “Azimuthal multiplexing 3d diffractive optics,” Scientific reports **10**, 1–9 (2020).

[69] Oussama Korichi, Markus Hiekkämäki, and Robert Fickler, “Complex modulation of light in polarization and space using laser-written multi-plane light conversion,” in *International Conference on Metamaterials, Photonic Crystals and Plasmonics* (2025) pp. 398–399.